Electronic Supplementary Material (ESI) for Inorganic Chemistry Frontiers.

Supporting Information

A Hybrid Halide Lead-Free Pseudo-Perovskite with Large Birefringence

Weiqi Huang,[a,c] Xiaolong Wu,[a,c] Belal Ahmed,[e] Yanqiang Li,[c] Yang Zhou,[c] Han Wang,[c] Yipeng Song,[c] Xiaojun Kuang,[b] Junhua Luo,[c,d] and Sangen Zhao[c,d,*]

[a]College of Chemical Engineering, Fuzhou University, Fuzhou 350116, China

[b]College of Materials Science and Engineering, Guilin University of Technology, Guilin 541004, China

[c]State Key Laboratory of Structural Chemistry, Fujian Institute of Research on the Structure of Matter, Chinese Academy of Sciences, Fuzhou 350002, China

[d]Fujian Science & Technology Innovation Laboratory for Optoelectronic Information of China, Fuzhou 350108, China

[e]Department of Chemistry, Shahjalal University of Science and Technology, Sylhet-3114, Bangladesh.

CONTENTS

Structure Determination.

A suitable colorless crystal of $MLASnCl_4$ (0.12 × 0.10 × 0.06 mm^3) was selected for single-crystal X-ray diffraction (SCRD) data collection. The SCRD diffraction data was collected on a Bruker D8 diffractometer using Mo Kα radiation (λ = 0.71073 Å) at 298.4(3) K. The data reduction and absorption corrections were carried out with the program APEX3. The crystal structure was solved by the direct method with the program SHELXS and refined with the least-squares program SHELXL.[1] Final refinement included anisotropic displacement parameters. The structure was checked for the symmetry elements using the program PLATON,[2] and no higher symmetry was found. Details of crystallographic parameters, data collection, and structure refinement are summarized in Table S1. The atomic coordinates and equivalent isotropic displacement parameters are listed in Table S2. The selected bond distances and angles are given in Table S3 and Table S4, and the anisotropic displacement parameters are presented in Table S5.

Powder X-ray diffraction Analysis.

Powder X-ray diffraction (PXRD) measurement for the sample of $MLASnCl_4$ was carried out with a Miniflex 600 diffractometer equipped with an incident beam monochromator set of Cu Kα radiation (λ = 1.5418 Å), and the 2θ range of 5-70°, with a scan step width of 0.02° and a scanning rate of 3° min^{-1} (Figure S2).

Elemental Analysis.

Semiquantitative microprobe analyses on the $MLASnCl_4$ crystal were performed with the aid of a field emission scanning electron microscope (Nova NanoSEM 230) equipped with an energy-dispersive X-ray spectroscope (EDS). The energy dispersive spectra were collected on visibly clean surfaces of the samples and confirmed the presence of Sn, Cl, C,

and N elements in an average ratio of Sn:Cl = 1:4.25, which is well consistent with that determined by single-crystal XRD analysis (Figure S3).

Thermal Stability.

The thermal stability was investigated by the differential thermal analysis (DTA) on a simultaneous NETZSCH STA 449C thermal analyzer in an atmosphere of flowing N_2. About 8.25 mg $MLASnCl_4$ powders were placed into an Al_2O_3 crucible, and heated at a rate of 10 $K \cdot min^{-1}$ from room temperature to 800 K (Figure S4).

UV-Vis-NIR Diffuse Reflectance Spectroscopy.

The UV-Vis-NIR diffuse reflection data were recorded at room temperature using a powdered $BaSO_4$ sample as a standard (100% reflectance) on a PerkinElmer Lamda-950 UV/Vis/NIR spectrophotometer. The scanning wavelength range is 200 to 800 nm (Figure S5). Absorption (K/S) data were calculated by Kubelka-Munk function:[3]

$F(R) = (1-R)^2/(2R) = K/S$

Where R is the reflectance, K is the absorption, and S is the scattering. In the (K/S) versus E plot, extrapolating the linear portion of the rising curve to zero gives rise to the onset of absorption.

IR Analysis.

Infrared spectroscopy (IR) in the wavenumber range of 4000–500 cm^{-1} was recorded on the Bruker Vertex 70 infrared spectrometer.

Birefringence Measurements.

The birefringence of $MLASnCl_4$ was characterized by using the polarizing microscope (NIKON ECLIPSE LV100N POL) equipped with a Berek compensator. The wavelength of the light source was 550 nm. Owing to the clear boundary lines of the first-, second-, and third-order interference color, the relative error was small enough. Before the scanning, the small and transparent $MLASnCl_4$ lamellar crystal was chosen to measure, to improve the accuracy of the birefringence. The thickness of the selected crystal was measured on the polarizing microscope.

The formula for calculating the birefringence is listed below,

$$R = | n_e - n_o | \times T = \Delta n \times T$$

Here, R represents the optical path difference, Δn means the birefringence, and T denotes the thickness of the crystal.

Computational Methods.

The first-principles calculations of electronic structure, band structure, and optical properties of $MLASnCl_4$ were carried out by using the CASTEP software[4] to understand the relationship between structure and properties. The generalized gradient approximation (GGA) was adopted, and Perdew-Burke-Ernzerhof (PBE) functional was chosen to calculate the exchange-correlation potential,[5,6] with an energy cutoff of more than 750 eV for $MLASnCl_4$. The Brillouin zone was sampled using the Monkhorst-Pack k-point sampling of 2×8×3. First of all, the atomic positions in the unit cell have been fully optimized using the GGA method with an energy cutoff of 1400 eV convergence to 10^{-7} eV. The band structure and density of states (DOS)/partial DOS were computed based on the energy convergence to 10^{-6} eV and 10^{-7} eV, respectively. The linear optical properties were examined based on the dielectric function $\varepsilon(\omega) = \varepsilon_1(\omega) + i\varepsilon_2(\omega)$. The imaginary part

of the dielectric function ε_2 can be calculated based on the electronic structures and the real part is obtained by the Kramers-Kronig transformation, accordingly, the refractive indices and the birefringence (Δn) can be calculated. The frequency-dependent refractive indices were calculated to demonstrate the validity of birefringence measurements.

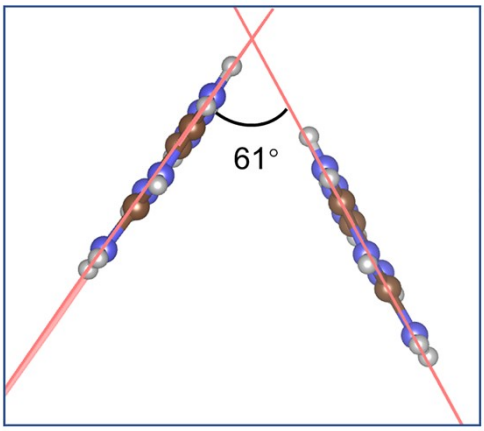

Figure S1. The observed dihedral angle in the compound between melamine cationic planes.

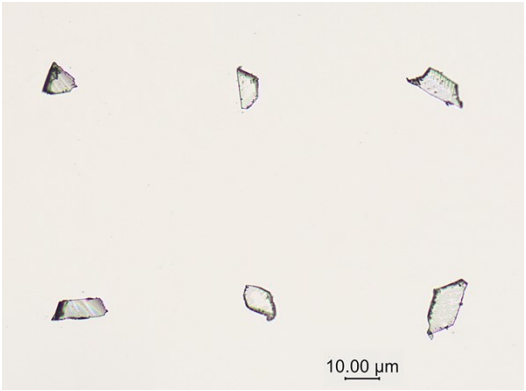

Figure S2. The photograph of the synthesized colorless transparent single crystals.

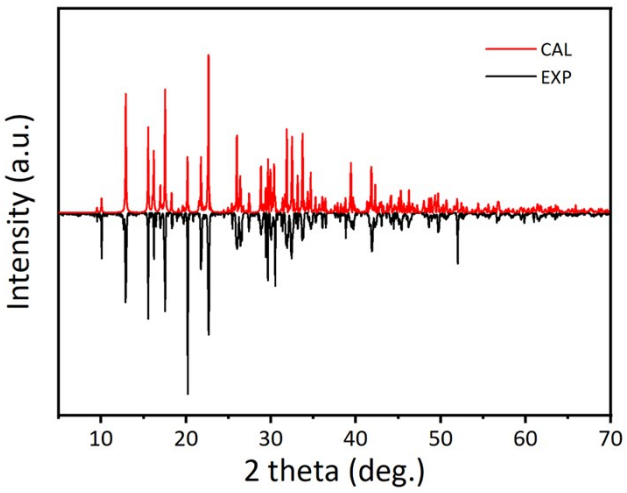

Figure S3. Experimental and calculated PXRD patterns of $MLASnCl_4$.

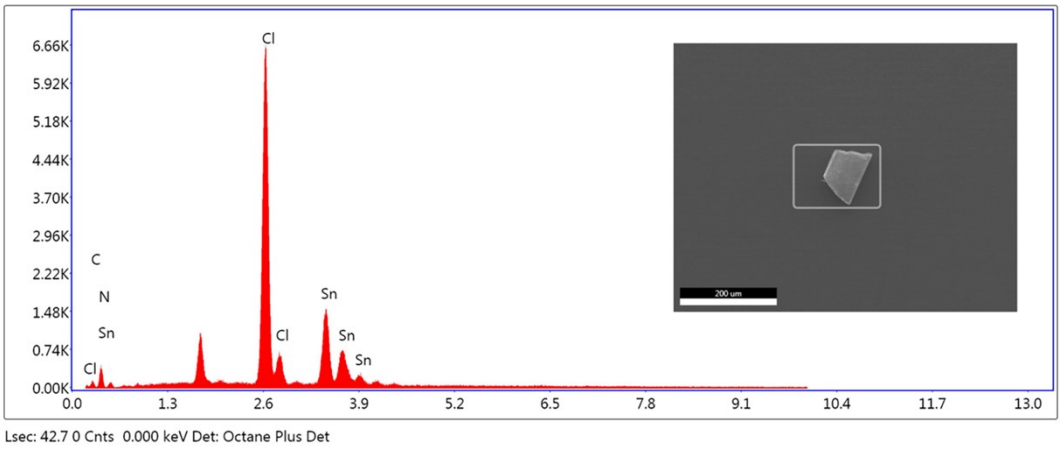

Figure S4. Energy dispersive X-ray (EDX) analysis of $MLASnCl_4$.

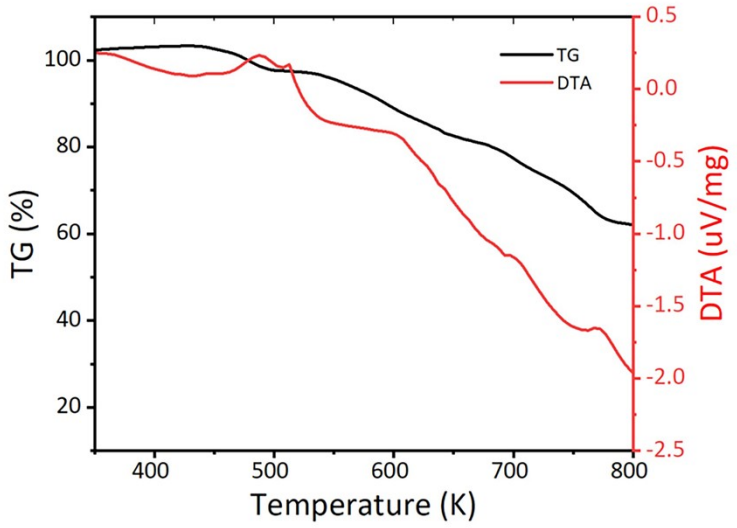

Figure S5. TG and DTA diagrams of $MLASnCl_4$.

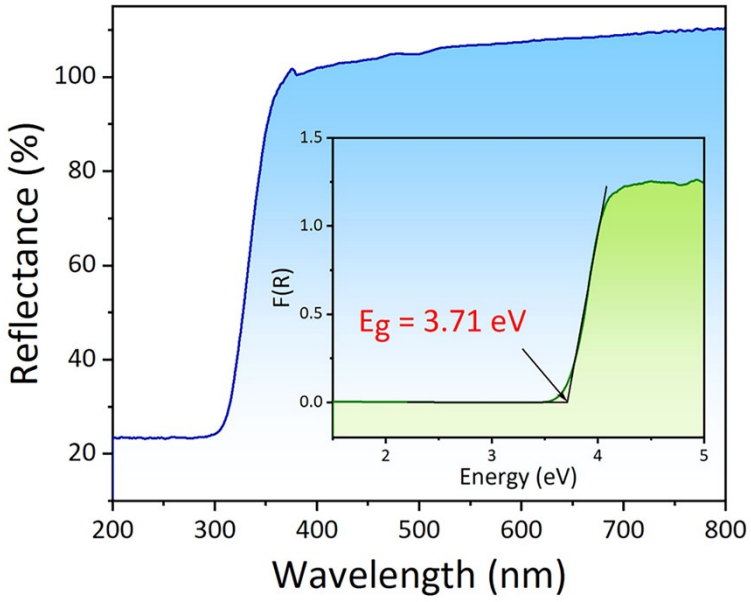

Figure S6. UV-vis-NIR-infrared diffuse reflectance spectrum of $MLASnCl_4$.

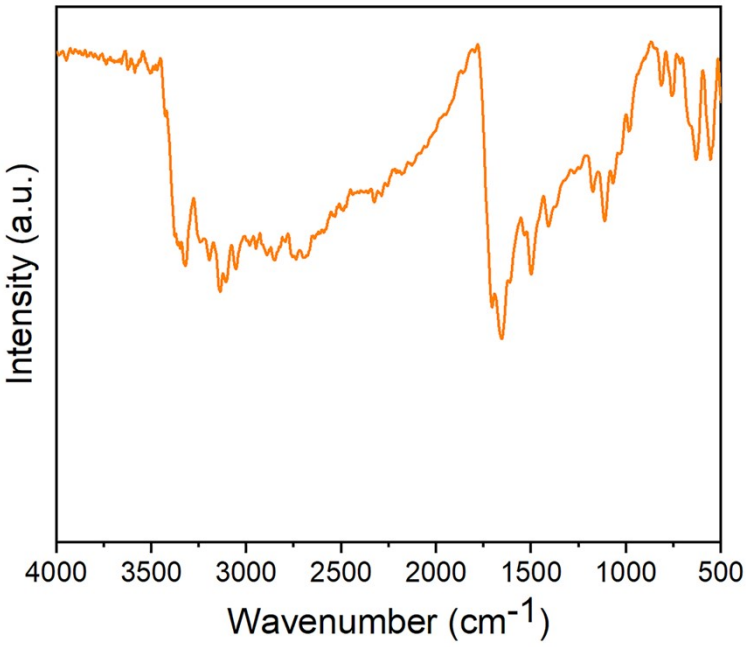

Figure S7. IR spectrum of $MLASnCl_4$.

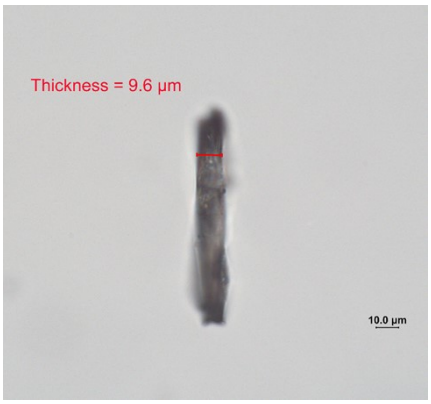

Figure S8. The thickness of the selected $MLASnCl_4$ crystal plate.

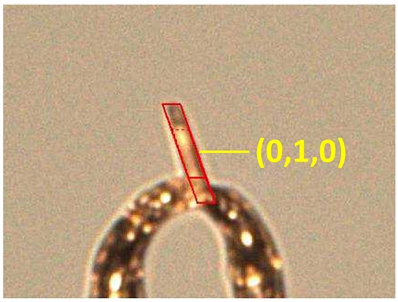

Figure S9. The crystal orientation of the selected $MLASnCl_4$ plate determined by single-crystal XRD.

Table S1. Crystallographic data and structure refinement for $MLASnCl_4$.

Empirical formula	$C_3N_6H_8SnCl_4$
Formula weight	388.64
Temperature (K)	298.4(3)
Crystal system, space group	Orthorhombic, *Pna*2_1
a (Å)	21.8661(7)
b (Å)	6.0217(2)
c (Å)	17.5955(5)
$\alpha/^O$	90
$\beta/^O$	90
$\gamma/^O$	90
Volume ($Å^3$)	2316.82(13)
Z	8
ρ_{calc} (g/cm^3)	2.228
μ (mm^{-1})	3.100
F(000)	1488.0
Crystal size (mm)	0.12 × 0.10 × 0.06
Theta range for data collection (deg.)	3.726 to 58.52
Limiting indices	$-27\leq h\leq 22$, $-4\leq k\leq 7$, $-22\leq l\leq 15$
Reflections collected	7389
Independent reflections	3870 [R_{int} = 0.0232, R_{sigma} = 0.0369]
Data/restraints/parameters	3870/1/254
Goodness-of-fit on F^2	1.025
Final R indices [I>2sigma(I)][a]	R_1 = 0.0329, wR_2 = 0.0824
R indices (all data)	R_1 = 0.0382, wR_2 = 0.0852
Largest diff. peak and hole($e.A^{-3}$)	1.69/-1.12

[a] $R_1 = \Sigma||F_o| - |F_c||/\Sigma|F_o|$ and $wR_2 = [\Sigma w(F_o^2 - F_c^2)^2/\Sigma wF_o^4]^{1/2}$ for $F_o^2 > 2\sigma(F_o^2)$.

Table S2. Atomic coordinates ($\times 10^4$) and equivalent isotropic displacement parameters ($Å^2 \times 10^3$) for $MLASnCl_4$.

Atom	*x*/a	*y*/b	*z*/c	U_{eq} [a]
Sn1	7298.7(2)	1901.9(8)	3377.6(3)	25.63(13)
Sn2	5157.4(2)	6846.5(8)	6625.5(2)	25.52(13)
Cl1	8190.4(8)	1912(3)	4471.5(12)	34.6(5)
Cl2	5179.5(8)	11011(4)	6485.1(14)	39.8(5)
Cl3	4262.2(8)	7011(4)	5517.5(13)	34.3(4)
Cl4	5843.9(8)	6090(4)	5444.1(11)	34.2(4)
Cl5	7276.1(8)	6037(4)	3584.6(13)	36.5(5)
Cl6	6378.2(12)	7231(4)	7366.4(14)	41.7(5)
Cl7	6095.0(10)	2405(4)	2616.9(15)	37.2(5)
Cl8	6617.5(8)	1076(4)	4539.4(11)	34.6(4)
C1	2181(4)	12288(15)	6319(5)	23.6(16)
C2	3205(3)	11981(13)	6473(4)	26.3(17)
C3	4777(3)	949(13)	4201(4)	24.7(15)
C4	4245(3)	-1835(12)	3520(4)	25.9(17)
C5	5269(4)	-2182(16)	3685(6)	26.7(17)
C6	2680(3)	9160(12)	5794(4)	24.6(15)
N1	4785(3)	2758(14)	4596(6)	36(2)
N2	1658(3)	13300(11)	6424(4)	36.2(18)
N3	5794(3)	-3205(11)	3572(4)	36.7(18)
N4	3720(3)	-2549(12)	3274(5)	35.4(19)
N5	3726(3)	12727(13)	6724(5)	38(2)
N6	5286(2)	-251(12)	4090(4)	27.3(14)
N7	3195(2)	9939(10)	6106(3)	25.9(13)
N8	4753(3)	-3008(11)	3414(4)	27.7(13)
N9	2165(3)	10344(11)	5900(4)	27.3(14)
N10	2694(2)	13128(10)	6577(4)	27.7(14)
N11	2672(3)	7333(16)	5401(6)	39(2)
N12	4261(2)	186(10)	3896(3)	25.8(12)

[a] U_{eq} is defined as one-third of the trace of the orthogonalized U_{ij} tensor.

Table S3. Selected bond distances (Å) for $MLASnCl_4$.

Sn1-Cl1	2.740(2)	N6-C3	1.341(9)
Sn1-Cl8	2.5779(19)	N6-C5	1.365(11)
Sn1-Cl5	2.517(2)	N8-C4	1.329(9)
Sn1-Cl7	2.968(2)	N8-C5	1.323(10)
Sn2-Cl4	2.6042(19)	N10-C2	1.326(9)
Sn2-Cl6	2.980(3)	N12-C4	1.386(9)
Sn2-Cl2	2.521(2)	N12-C3	1.331(9)
Sn2-Cl3	2.764(2)	N3-C5	1.317(10)
N1-C3	1.292(11)	N7-C6	1.339(9)
C1-N10	1.312(10)	N7-C2	1.388(10)
C1-N2	1.308(10)	C6-N9	1.345(9)
C1-N9	1.384(11)	C6-N11	1.300(11)
N4-C4	1.298(10)	C2-N5	1.302(10)

Table S4. Selected bond angles (deg.) for $MLASnCl_4$.

Cl1-Sn1-Cl7	161.37(7)	C3-N12-C4	121.2(6)
Cl8-Sn1-Cl1	81.64(6)	N4-C4-N8	121.0(7)
Cl8-Sn1-Cl7	82.23(7)	N4-C4-N12	118.3(7)
Cl5-Sn1-Cl1	84.84(6)	N8-C4-N12	120.7(6)
Cl5-Sn1-Cl8	93.71(7)	C6-N7-C2	120.9(6)
Cl5-Sn1-Cl7	86.96(6)	N7-C6-N9	117.5(6)
Cl4-Sn2-Cl6	81.17(6)	N11-C6-N7	121.7(6)
Cl4-Sn2-Cl3	81.46(6)	N11-C6-N9	120.8(6)
Cl2-Sn2-Cl4	94.87(7)	C6-N9-C1	120.1(6)
Cl2-Sn2-Cl6	87.04(6)	N1-C3-N6	121.5(7)
Cl2-Sn2-Cl3	84.77(7)	N1-C3-N12	121.3(7)
Cl3-Sn2-Cl6	160.07(7)	N12-C3-N6	117.3(7)
N10-C1-N9	122.1(7)	N10-C2-N7	120.8(7)
N2-C1-N10	121.3(8)	N5-C2-N10	120.6(7)
N2-C1-N9	116.5(7)	N5-C2-N7	118.5(7)
C3-N6-C5	120.9(7)	N8-C5-N6	122.0(7)

C5-N8-C4	117.7(7)	N3-C5-N6	117.0(8)
C1-N10-C2	118.2(7)	N3-C5-N8	120.9(8)

Table S5. Anisotropic displacement parameters ($Å^2$) for $MLASnCl_4$.

Atom	U_{11}	U_{22}	U_{33}	U_{23}	U_{13}	U_{12}
Sn1	28.0(2)	23.9(3)	24.9(2)	-2.0(2)	2.0(2)	0.69(18)
Sn2	28.3(2)	22.4(3)	25.9(2)	0.0(3)	1.9(2)	-0.61(18)
Cl1	29.3(8)	39.2(14)	35.2(10)	9.5(9)	-2.6(8)	-6.5(8)
Cl2	31.5(8)	22.4(11)	65.7(17)	0.0(10)	-1.5(9)	-1.1(8)
Cl3	29.1(8)	39.4(13)	34.5(10)	-9.3(9)	-2.4(8)	7.3(8)
Cl4	28.2(7)	46.0(13)	28.4(8)	1.6(8)	1.6(7)	8.3(8)
Cl5	32.6(8)	24.1(11)	52.7(13)	-1.6(8)	-4.1(8)	0.7(8)
Cl6	59.2(13)	30.9(13)	35.0(14)	5.3(8)	0.9(11)	-0.6(10)
Cl7	51.5(11)	26.7(12)	33.3(12)	-2.2(8)	-2.4(10)	3.7(9)
Cl8	27.8(7)	47.7(13)	28.4(8)	-0.8(8)	0.3(7)	-7.1(8)
C1	26(3)	24(4)	21(4)	-2(3)	2(4)	1(3)
C2	26(3)	27(5)	26(4)	4(3)	-2(3)	6(3)
C3	36(3)	19(4)	19(3)	0(3)	-3(3)	3(3)
C4	29(3)	22(4)	27(4)	4(3)	-3(3)	0(3)
C5	27(3)	31(5)	22(4)	-1(3)	5(3)	3(3)
C6	31(3)	21(4)	22(3)	3(3)	0(3)	3(3)
N1	39(4)	30(5)	39(5)	-8(3)	-12(3)	6(3)
N2	25(3)	43(5)	41(4)	-10(3)	1(3)	8(3)
N3	28(3)	44(5)	38(4)	-9(3)	0(3)	9(3)
N4	30(3)	21(4)	55(6)	-9(3)	-8(4)	2(3)
N5	32(3)	32(4)	50(6)	-6(3)	-17(4)	0(3)
N6	24(3)	28(4)	29(3)	-8(3)	-4(3)	1(3)
N7	24(2)	22(3)	31(3)	-2(3)	-5(2)	8(3)
N8	29(3)	26(4)	28(3)	-5(3)	-4(3)	3(2)
N9	24(2)	27(4)	31(3)	-5(3)	-3(3)	-2(3)
N10	27(3)	29(4)	27(3)	-3(3)	1(3)	3(2)
N11	44(4)	34(5)	41(5)	-15(4)	-3(4)	7(3)
N12	27(3)	19(3)	31(3)	-1(3)	-1(2)	8(3)

Table S6. The bond valence sum (BVS) for all atoms in [$SnCl_4$] unit for MLA$SnCl_4$. The bond valences for each atom in [$SnCl_4$] unit are calculated according to the following equation: bond valence = exp[(R_o-R)/B], where R is the bond length. The bond valence parameter is as follow: R_o(Sn-Cl) = 2.36 Å, B(Sn-Cl) = 0.37 Å.[7]

Sn1	1.76	Cl4	0.63
Sn2	1.69	Cl5	0.65
Cl1	0.59	Cl6	0.64
Cl2	0.65	Cl7	0.63
Cl3	0.61	Cl8	0.61

References

(1) G. M. Sheldrick, A short history of SHELX, *Acta Crystallogr. Sect. A: Found. Crystallogr.* **2008**, *64*, 112-122.

(2) A. L. Spek, Single-crystal structure validation with the program PLATON, *J. Appl. Crystallogr.* **2003**, *36*, 7-13.

(3) J. Tauc, Absorption Edge and Internal Electric Fields in Amorphous Semiconductors, *Mater. Res. Bull.* **1970**, *5*, 721.

(4) G. Kresse, J. Furthmuller, Efficient iterative schemes for *ab initio* total-energy calculations using a plane-wave basis set, *Phys. Rev. B.* **1996**, *54*, 11169-11186.

(5) J. P. Perdew, K. A. Jackson, M. R. Pederson, D. J. Singh, C. Fiolhais, Erratum: Atoms, molecules, solids, and surfaces: Applications of the generalized gradient approximation for exchange and correlation, *Phys. Rev. B.* **1993**, *46*, 6671.

(6) J. P. Perdew, K. Burke, M. Ernzerhof, Generalized Gradient Approximation Made Simple, *Phys. Rev. Lett.* **1996**, *77*, 3865.

(7) I. D. Brown, D. Altermatt, Bond-valence parameters obtained from a systematic analysis of the Inorganic Crystal Structure Database, *Acta Crystallogr., Sect. B: Struct. Sci.*, **1985**, *41*, 244-247.